EXPERIMENTAL VERIFICATION OF DISPERSIVE WAVE PROPAGATION ON GUITAR STRINGS

Dmitri Kartofelev
Tallinn University of Technology,
School of Science,
Department of Cybernetics,
Tallinn, Estonia
dima@ioc.ee

Joann Gustav Arro
Tallinn University of Technology,
School of Science,
Department of Cybernetics,
Tallinn, Estonia
joann.arro@taltech.ee

Vesa Välimäki
Aalto University,
School of Electrical Engineering,
Department of Signal Processing and
Acoustics, Acoustics Lab,
Espoo, Finland
vesa.valimaki@aalto.fi

ABSTRACT

Experimental research into the fundamental acoustic aspects of musical instruments and other sound generating devices is an important part of the history of musical acoustics and of physics in general. This paper presented experimental proof of dispersive wave propagation on metal guitar strings. The high resolution experimental data of string displacement are gathered using video-kymographic high-speed imaging of the vibrating string. The experimental data are indirectly compared against a dispersive Euler-Bernoulli type model described by a PDE. In order to detect the minor wave features associated with the dispersion and distinguish them from other effects present, such as frequency-dependent dissipation, a second model lacking the dispersive (stiffness) term is used. Unsurprisingly, the dispersive effects are shown to be minor but definitively present. The results and methods presented here in general should find application in string instrument acoustics.

1. INTRODUCTION

Modern acoustic guitar strings are made of different metal alloys. Metal string produces a different sound to nylon or gut strings. Guitar strings may be "plain", consisting only of a single material, like steel, nylon, or gut. Also they may be wound, having a core of one material and an overwinding of another.

Usually, plain guitar strings are not associated with significant dispersive effects like e.g. the bulkier steel piano strings are [1]. Thin guitar strings have a relatively low bending stiffness. The aim of this paper is to experimentally investigate and prove the possibility of transverse dispersive wave propagation on the second and third strings used in acoustic guitars.

Several models of transverse wave propagation on a stiff string, of varying degrees of complexity, have appeared in the literature [2–6]. Models with great emphasis on realistic frequency-dependence loss profiles are [7, 8]. These

models, intended for the synthesis of musical tones, are always framed in terms of a partial differential equation (PDE), or a system of PDEs. The simplified starting point for such models is the one-dimensional wave equation [9]. More realistic features, such as dispersion, various nonlinearities and frequency-dependent losses, are incorporated through several extra terms. Discussion in this paper is informed by the model equation proposed by Bensa *et al.* in [6], i.e., Euler-Bernoulli.

Some direct measurements of string vibration have been previously conducted. The methods of string displacement measurement can be roughly divided into three categories: the electromagnetic methods, electric field sensing, and optical methods. The electromagnetic methods exploit Faraday's law, and the principle of the string displacement detection is the following: An electromagnetic coil is placed near the string, and the motion of the string induces a voltage in the circuit that is proportional to the string's velocity from which the displacement of the string is obtained. This method was used and described in [10].

The electric field sensing makes use of the phenomenon of capacitance change between two electrodes, when the distance between them is varied. In the simplest approach, a conducting string is grounded, and direct current (DC) voltage is applied to an electrode plate. The string's movement modulates the voltage between the string and the plate, and the information about the string's displacement is obtained *cf.* [11].

The optical methods exploit various light or laser emitting and detecting sensors to capture vibration. For example, high speed cameras with suitable video analysis have been used to measure string vibration successfully [12]. Also, different devices that convert laser light into a uniform parallel beam and detect their shadows can ensure the result [13]. Devices that are based on various photovoltaic detectors have also been successful [14].

Our experimental approach can be classified under the aforementioned optical methods. We use a non-invasive video-kymographic method based on the exploitation of a digital high-speed line-scan camera (LSC) imaging. The method has been used successfully in musical acoustics research [15–17]. A monochord equipped with a guitar string is measured [1]. Experimentally obtained string vibration

---

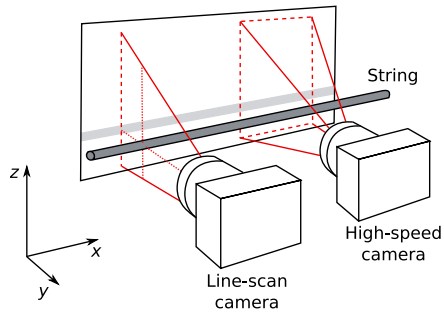[1] String set: Earthwood Light 2148. String gauge: 0.015 (15, 1115).

Figure 1. Operating principle of the LSC compared to an ordinary high-speed camera. Geometry of the area that is being imaged is shown on the white screen with the dashed red lines. Placement of the LSC with respect to the string vibrating in the z-direction while recording the vibration.
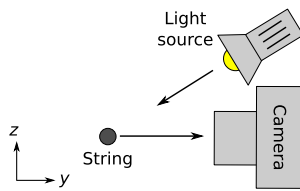

Figure 2. LSC recording string displacement. Cross-section of the recorded string is shown with the grey bullet.

data are then compared directly or indirectly against theoretical models, expanded upon below, with the aim to deduce some beneficial observations and reach conclusions.

Organisation of the paper is the following: Sec. 2 explains the experimental approach and set-up; Sec. 3 presents the dispersion analysis of the dispersive Euler-Bernoulli type model [6]. Numerically integrated solution of this model is presented and compared against its dispersion analysis; Sec. 4 presents a simpler time-stepping model of lossy non-dispersive string vibration, that is used here to identify dispersive features present in experimental data, and to distinguish them from other effects, such as frequency-dependent dissipation; Sec. 5 presents the experimental results and compares them against our assumptions and presented theory (the simplified model). Analysis and discussion of the results is directly informed by the Euler-Bernoulli type model; Sec. 6 concludes the paper.

2. EXPERIMENTAL MEASUREMENTS

The string displacement is measured using a LSC. The camera produces two-dimensional digital images (not videos) called the *kymographs*. The geometry of a digital imaging sensor of the LSC differs from a commonly used video camera. Usually, the video camera sensor pixels are placed in rows and columns forming a grid. The LSC sensor consists only of a single pixel array, referred here to, as the *line*, see Fig. 1. While filming the camera continuously stacks these lines to form an image. In addition, the global shutter technology allows for all pixels in a line to work

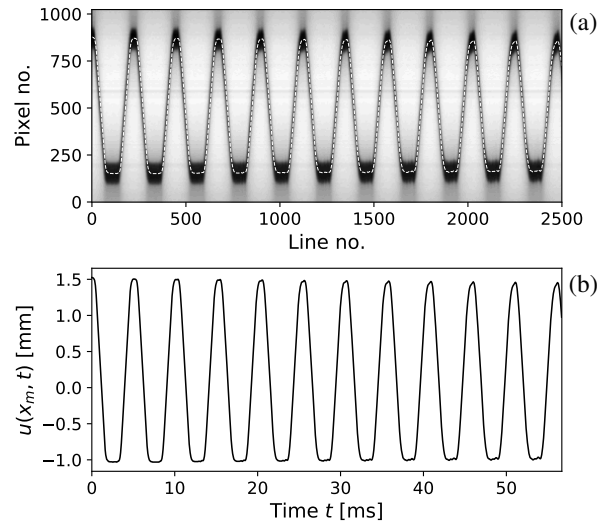Manufacturer: Ernie Ball Inc. Coachella, California, USA 92236

Figure 3. (a) Kymograph of vibrating string. Image recorded at $44\,100$ lines/s. String displacement $u(x_m, t)$ tracking with line convolution method (2) is shown with the overlaid dashed line. (b) Calibrated string displacement time-series corresponding to the kymograph above.
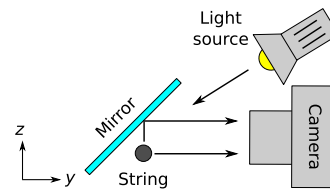

Figure 4. Dual polarisation measurement set-up [15].

as one (collect light simultaneously), preventing any image distortions to influence the recordings. Figures 1 and 2 show the perpendicular placement of the LSC with respect to the string while recording.

The string displacement time-series extraction from a kymograph is based on the discrete one-dimensional convolution integral of the individual kymograph lines

$$c[i] = (p * k)[i] = \sum_{n=-\infty}^{\infty} p[n]\, k[i - n], \qquad (1)$$

where $i \in [1, 1024]$ is the pixel number in any given line, $p[i]$ is the image depth or colour value in bits, and $k[i]$ is the convolution kernel — the image feature we are interested in. The kernel is selected to be roughly similar in shape to the string (its image), this guarantees that the convolved line $c[i]$ will have a clear maximum (or minimum) that will coincide with the string position [16]. Thus, for any given line the pixel corresponding to string position

$$i = \arg\max c[i] \quad (\text{or } i = \arg\min c[i]). \qquad (2)$$

This procedure is repeated for all kymograph lines. Figure 3a shows an example kymograph and the result of the image analysis. Figure 3b shows the calibrated time-series where the line number is multiplied by $dt = 1/44\,100$ s since the camera is recording at audio sampling rate of
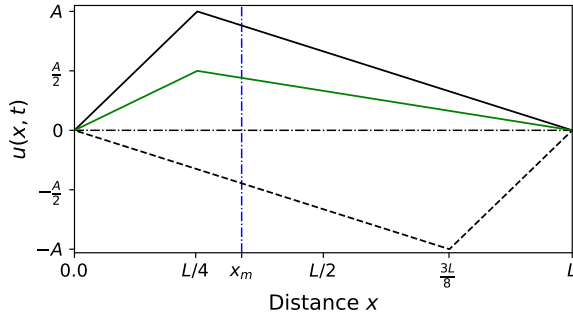
Figure 5. Schematic of the problem studied. Triangular shaped initial condition exited at $x = x_e = L/4$ is shown with the solid black line, and the corresponding traveling waves (overlapping) are shown with the green line. The dashed line shows the string displacement at one half of the period. Vertical dash-dotted line shows the measurement coordinate $x = x_m$ used in the experiment.

44 100 lines/s, and the pixel number i is multiplied by dx which value is determined by filming an object (high-contrast calibration sheet) with known dimensions.

2.1 Proof of planar vibration

In case a dual-polarisation measurement is required the LSC is used in combination with a mirror. The mirror is placed behind the string under a 45° angle with respect to the optical axis of the camera, as shown in Fig. 4. One half of the kymograph will contain displacement data for the vertical z-axis, and the other half for the horizontal y-axis.

The following method of controlled and repeatable string excitation is used in this study. The method is based on the fact that a thin cotton thread, when under great tensile load, snaps quite rapidly when heated abruptly (burned with a flame). The thread is looped around the string at the desired excitation point $x = x_e$ along the string's speaking length, the string is then displaced to a suitable initial amplitude A in the desired direction with respect to the LSC. This procedure creates a triangular shaped initial condition shown in Fig. 5. Figure 6 shows that the guitar string exited in such a manner is capable of sustained planar vibration. At least for *some* time after the excitation.

3. DISPERSIVE STRING MODEL

The planar transverse vibration of a lossy stiff string can be described by

$$\frac{\partial^2 u}{\partial t^2} = c^2 \frac{\partial^2 u}{\partial x^2} - \gamma^2 \frac{\partial^4 u}{\partial x^4} - 2\alpha \frac{\partial u}{\partial t} + 2\beta \frac{\partial^3 u}{\partial x^2 \partial t}, \quad (3)$$

where $u(x,t)$ is the string displacement in z-direction and the non-negative α, β, γ and c are the system parameter. The first term on the right-hand side of the equation, in the absence of the others, gives rise to ideal wave vibration, with traveling wave speeds c [9]. The second term introduces dispersion and is responsible for frequency-dependent wave velocity where constant γ is proportional to the bending stiffness. Last two terms allow for losses, and if $\beta \neq 0$, decay rates are frequency-dependant.
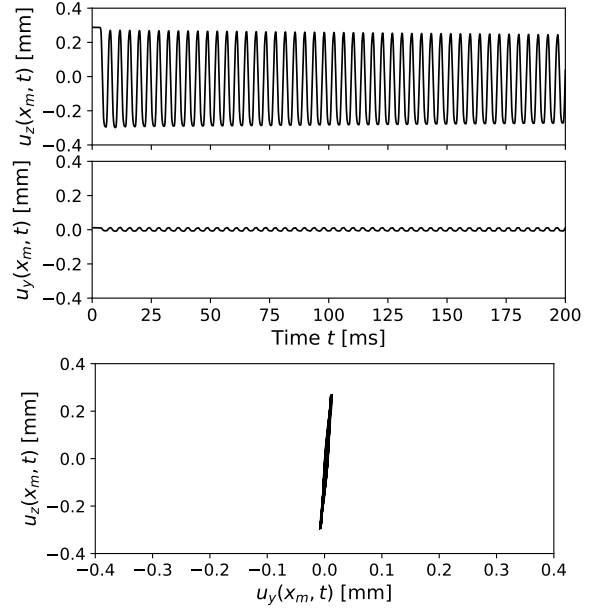

Figure 6. Persistent planar vibration. String displacement u is recorded at $x = x_m$ using the measurement set-up shown in Fig. 4. Subscripts y and z indicate the direction of vibration as shown in Figs. 1 and 4.

3.1 Dispersion analysis and characteristic equation

The solution to Eq. (3) is assumed in the form

$$u \simeq u_0 e^{\varsigma t + i\kappa x}, \quad (4)$$

where the complex frequency $\varsigma = \varsigma(\kappa)$ is a function of wavenumber κ and $\kappa \in \mathbb{R}^+$, i is the imaginary unit, and u_0 is an initial amplitude. Solving the characteristic equation

$$\varsigma^2 + 2q(\kappa)\varsigma + r(\kappa) = 0, \quad (5)$$

where

$$q(\kappa) = \beta\kappa^2 + \alpha, \quad r(\kappa) = c^2\kappa^2 + \gamma^2\kappa^4, \quad (6)$$

for ς gives

$$\varsigma_\pm = -q \pm \sqrt{q^2 - r}. \quad (7)$$

These roots determine the behaviour of the general solution (4) of Eq. (3). Condition that the initial value problem corresponding to Eq. (3) be well posed is that roots (7) have real parts which are bounded from above as a function of κ; this is to say that solution growth can be no faster than exponential, see assumption (4). Another physically relevant condition is that roots (7) have non-positive real parts for all κ, so that all exponential solutions are non-increasing (infinite string displacement). This condition is satisfied because $q(\kappa) > 0$, $r(\kappa) > 0$ for positive κ. We rewrite the complex frequency using new variables

$$\varsigma = \text{Re}(\varsigma) + \text{Im}(\varsigma) = \sigma + i\omega. \quad (8)$$

Substituting (8) into general solution (4) gives

$$u \simeq u_0 e^{(\sigma+i\omega)t + i\kappa x} = u_0 e^{\sigma t} e^{i(\omega t + \kappa x)}, \quad (9)$$
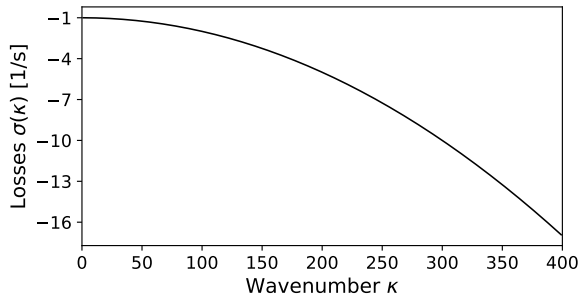
Figure 7. Losses $\sigma(\kappa)$ corresponding to Eq. (3) shown for parameter values (12).
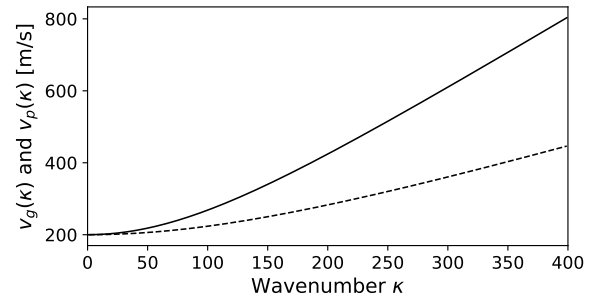

Figure 8. Group velocity, shown with the solid line, and phase velocity, shown with the dashed line, corresponding to Eq. (3) and calculated for parameter values (12).

from here it is easy to see that imaginary part of roots (7) corresponds to oscillation frequencies, and real part

$$\sigma(\kappa) = -q = -\alpha - \beta\kappa^2, \qquad (10)$$

to losses. Clearly, for real wavenumbers κ such that $q^2 \leq r$ imaginary part

$$\omega(\kappa) = \sqrt{q^2 - r} =$$
$$= \sqrt{-(\alpha + \beta\kappa^2)^2 + c^2\kappa^2 + \gamma^2\kappa^4} \neq 0, \quad (11)$$

and the resulting string vibration corresponds to normal damped wave propagation. For realistic values of parameters in (3), the condition $q^2 \leq r$ (traveling wave solution) holds for the vast majority of the audible frequency range. Also, notice that for $\alpha, \beta \geq 0$, loss $\sigma = -q$ depends on κ, the damping rates are wavenumber and thus frequency dependent, moreover, the losses increase as a function of κ. On the other hand, if $q^2 > r$, then both roots (7) are purely real and non-positive, yielding damped non-traveling solutions. A more detailed analysis of this model has been performed by Bensa *et al.* in [6].

In order to demonstrate the obtained analytic results realistic parameter values, taken from [6], for Eq. (3) are chosen as follows:

$$c \simeq 200 \, \frac{\mathrm{m}}{\mathrm{s}}, \;\; \gamma \simeq 1 \, \frac{\mathrm{m}^2}{\mathrm{s}}, \;\; \alpha \simeq 1 \, \frac{1}{\mathrm{s}}, \;\; \beta \simeq 10^{-4} \, \frac{\mathrm{m}^2}{\mathrm{s}}. \;\; (12)$$

These values correspond to a highly dispersive piano string rather than the guitar string considered below. In further discussion we are ignoring small wavenumber (extremely long wavelength) modes (in this case $\kappa \lesssim 0.760$)[2]. The behaviour for $\kappa \lesssim 0.760$ is most likely non-physical due to the heuristics of the manner in which Eq. (3) was derived. Additionally, wave motion related to these wave components is outside the audible range of wavenumbers.

Figure 7 shows the decay curve for the selected parameters (12). As expected the exponential decay rates become greater as a function of κ. Phase velocity $v_p(\kappa) = \omega/\kappa$ and group velocity $v_g(\kappa) = d\omega/d\kappa$ curves are shown in Fig. 8. For all $\kappa > 0$, $v_g > v_p$ which means that with the passage of time a pulse propagating on the string will distort in a manner such that a high-frequency oscillating tail will tend to appear in front of the pulse.
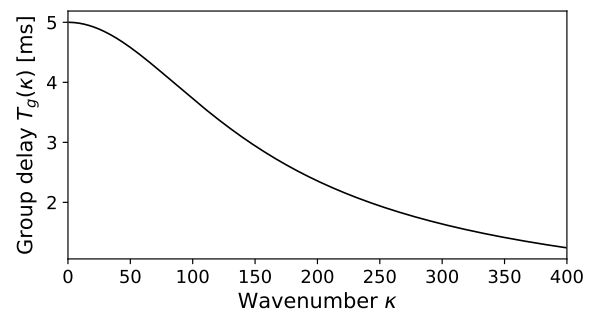

Figure 9. Group delay corresponding to Eq. (3) shown for parameter values (12).

This type of dispersion is referred to as the *anomalous* dispersion. The group delay, unit length multiplied by the inverse of the group velocity, shown in Fig. 9 also confirms that high-frequency wave components travel faster than the low-frequency ones. This behaviour can be confirmed by numerically integrating Eq. (3). The initial value problem is solved on an infinite half-plane $x \in (-\infty, \infty)$, $t \in [0, \infty)$ to eliminate any effects of wave interactions for $t \gg 1$ caused by the fast traveling high-frequency wave components reflecting from the edges of a finite integration domain. We select a bell-shaped initial condition

$$u(x, 0) = A \operatorname{sech}^2 \eta x = \frac{4Ae^{2\eta x}}{(1 + e^{2\eta x})^2}, \qquad (13)$$

where $A = 2$ mm is the string amplitude, $\eta = 2$ is the pulse width parameter. This parameter selection results in an approximately 2 m wide pulse — not too dissimilar from the realistic wavelengths found in string instruments. Figure 10 shows the integration result for parameter values (12) and for three space positions. The pulse evolution is exactly as predicted by the dispersion analysis. A dispersive high-frequency oscillating tail emerges in front of the main pulse by arriving earlier and becomes more prominent further the pulse propagates.

A careful look at the expressions of the phase and group velocities reveals that $\lim_{\kappa\to\infty} v_p = \infty$ and $\lim_{\kappa\to\infty} v_g = \infty$. These results are clearly not physical. In a realistic physically-sound models these curves should plateau out to some finite *dynamic* velocity value. One could fix this *problem* by adding appropriate small magnitude higher order terms to model (3). Once again, as in the case $\kappa \ll 1$,

---

[2] Criterion for determining the value: solve $dv_g/d\kappa = 0$ for $\kappa > 0$.
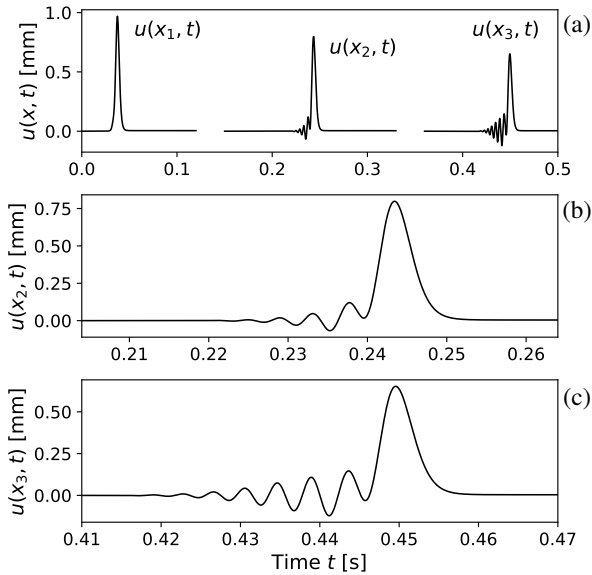
Figure 10. (a) Numerical integration of the initial value problem corresponding to Eq. (3), initial condition (13) and parameter values (12). Results are shown for space positions: $x_1 = \pm 7.50$ m, $x_2 = \pm 48.75$ m, $x_3 = \pm 90.00$ m. (b) Magnified pulse shape, case $x = x_2$. (c) Magnified pulse shape, case $x = x_3$.

we conclude that this behaviour is non-physical and luckily for us outside the audible range of frequencies.

4. NON-DISPERSIVE STRING MODEL

In order to identify the high-frequency and low-amplitude dispersive wave propagation in the experimental measurements presented below, we also consider a non-dispersive model with frequency-independent loss. The heuristics of our approach are directly determined by the d'Alembert formula (traveling wave solution). Modeling approach presented here is similar to [18, 19].

We consider vibration of a lossy ideal string described by wave equation

$$\frac{\partial^2 u}{\partial t^2} = c^2 \frac{\partial^2 u}{\partial x^2} - 2\alpha \frac{\partial u}{\partial t}, \qquad (14)$$

where $u(x,t)$ is the displacement, $c = \sqrt{T/\mu}$ is the speed of the waves traveling on the string, T is the tension and μ is the linear mass density (mass per unit length) of the string. In the context of a real string Eq. (14) can be used as an approximation of thin homogeneous elastic string vibration under a small amplitude restriction. In this case wave speed $c = \sqrt{T/(\rho A_\circ)}$, where ρ is the volumetric density, $A_\circ = \pi r^2$ is the cross-section area of a cylindrical string, and T is the tension. Second term on the right-hand side of (14) introduces frequency-independent loss, much the same way as in Eq. (3). It is easy to show that for $\alpha > 0$ all frequency components will decay $\sim e^{-\alpha t}$. As in the case (3), this term can be seen as a perturbation term acting on the wave equation in the following form:

$$\frac{\partial^2 u}{\partial t^2} = c^2 \frac{\partial^2 u}{\partial x^2}, \qquad (15)$$

thus its linear effects on the final solution can be added separately. For now we focus on Eq. (15). It is well known that Eq. (15) has an analytical solution. For infinite string (ignoring boundary conditions for now), for initial conditions $u(x,0) = u_0(x)$, and $\partial u(x,0)/\partial t = 0$ the solution takes the following form:

$$u(x,t) = \frac{1}{2}\left(u_0(x - ct) + u_0(x + ct)\right). \qquad (16)$$

This solution represents a superposition of two traveling waves: $u_0(x - ct)/2$ moving to the right (positive direction of the x-axis); and $u_0(x + ct)/2$ moving to the left. Function $u_0/2$ describes the shape of these waves and stays constant with respect to x-axis, as they are translated in opposite directions at speed c.

In general, a wave on any arbitrary segment of the string can be understood as a sum of two traveling waves that do not need to be equal. It can be written as

$$u(x,t) = r(x - ct) + l(x + ct), \qquad (17)$$

where $r(x - ct)$ is the traveling wave moving to the right and $l(x + ct)$ is the traveling wave moving to the left.

A well-known time-stepping method for implementing d'Alembert formula is the following. We discretise xt-plane into $n \times m$ discrete samples. We discretise the x-axis with grid spacing $\Delta x = L/n$ where L is the speaking length of the string, and the t-axis with grid spacing $\Delta t = t_{max}/m$, where t_{max} is the integration time. We let $x_i = i\Delta x$, where $0 \leq i \leq n$ and $t^j = j\Delta t$, where $0 \leq j \leq m$. From here it follows that $u_i^j = u(x_i, t^j)$, $r_i^j = r(x_i, t^j)$, and $l_i^j = l(x_i, t^j)$. And, by applying

$$r_i^{j+1} = r_{i-1}^j, \qquad (18)$$

$$l_i^{j+1} = l_{i+1}^j, \qquad (19)$$

for all grid points i and j in a sorted order one gets translation of numerical values r_i^j and l_i^j propagating in opposite directions with respect to the x_i-axis. This result agrees with d'Alembert formula (16) or (17) and can be understood as a digital waveguide based on traveling wave decomposition and use of two delay lines. The equivalence between the model used here and digital waveguide modeling is shown in [20].

So far we have not addressed the boundary conditions of Eq. (15). We assume that the string is fixed at both ends. The following boundary conditions apply:

$$u(0,t) = u(L,t) = 0, \quad t \in [0, t_{max}], \qquad (20)$$

where t_{max} is the desired integration time. By applying boundary conditions (20) to the general solution (17) The reflected traveling wave located at $x = 0$ can be found in the following form:

$$u(0,t) = r(-ct) + l(ct) = 0 \Rightarrow r(-ct) = -l(ct), \quad (21)$$

and similarly for $x = L$:

$$u(L,t) = r(L - ct) + l(L + ct) = 0 \Rightarrow$$
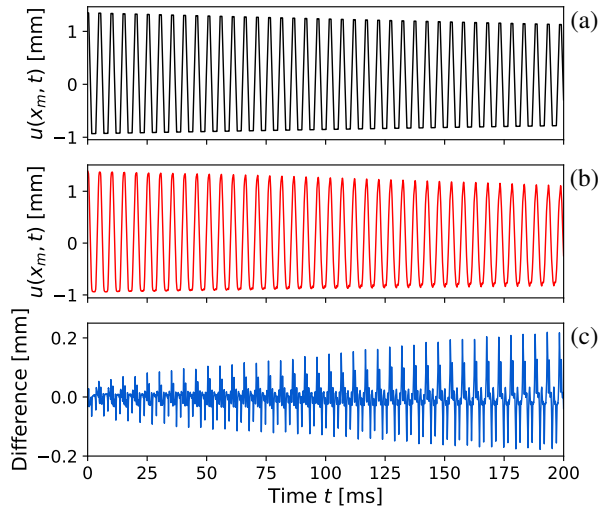$$\Rightarrow l(L + ct) = -r(L - ct). \qquad (22)$$

Figure 11. (a) Output of the model based on Eq. (14). (b) Experimental measurement. (c) Difference between model (14) and the experiment.
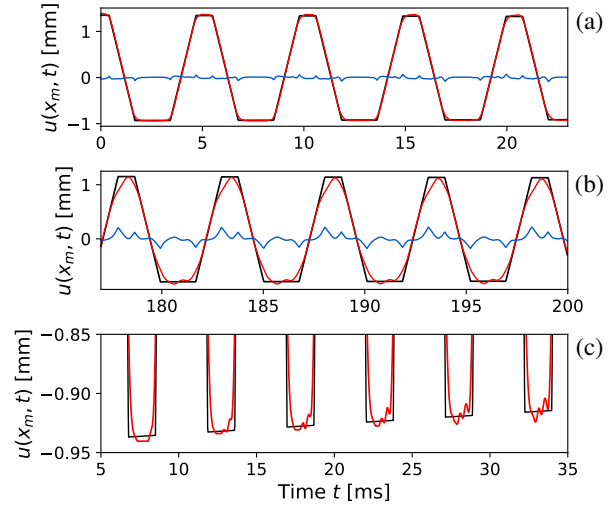

Figure 12. Magnified time-series of the results shown in Fig. 11. Model (14) output shown with the black line, the experiment shown with the red and the difference with the blue line. (a) First 25 ms of vibration. (b) Last 25 ms of vibration. (c) Magnification of the convex valleys of the signals shown in Fig. 11 displayed for $5 \leq t \leq 35$ ms.

These results are discretised according to the discretisation scheme discussed above. The traveling wave (21) reflected from the left boundary at $x = 0$ is

$$r_0^j = -l_0^j, \quad j \in [0, m], \tag{23}$$

and the traveling wave (22) reflected from the right boundary at $x = L$ is

$$l_n^j = -r_n^j, \quad j \in [0, m]. \tag{24}$$

In order to obtain the resulting string displacement u_i^j, for the selected initial and boundary conditions, a superposition of traveling waves (18), (19), (23), and (24) is found in accordance with general solution (17)

$$u_i^j = r_i^j + l_i^j, \quad i \in [0, n], \ j \in [0, m]. \tag{25}$$

Finally, there remains the question of loss introduced in (14). Since loss is $\sim e^{-\alpha t}$ in the continuous domain and in the discrete domain $\sim e^{-\alpha j \Delta t}$ we update (18) and (19) to

$$r_i^{j+1} = r_{i-1}^j e^{-\alpha j \Delta t / j} = r_{i-1}^j e^{-\alpha \Delta t}, \tag{26}$$

$$l_i^{j+1} = l_{i+1}^j e^{-\alpha j \Delta t / j} = l_{i+1}^j e^{-\alpha \Delta t}. \tag{27}$$

5. RESULTS AND DISCUSSION

Figure 5 shows the experimental set-up schematically. The following values of parameters were used: speaking length of the string $L = 0.65$ m; fundamental frequency $f_0 = 196.36$ Hz; excitation point for triangular initial condition $x = x_e = 0.25L = 0.163$ m; initial amplitude $A = 1.76$ mm; loss parameter $\alpha = 1.1$ s^{-1}. All time and frequency domain results are shown or calculated for string displacement $u(x_m, t)$ where measurement point $x_m = 0.41L = 0.266$ m. The spectrograms and power spectra are calculated using the Fast Fourier Transform algorithm. In calculating spectrograms a sliding window approach, in combination with the Hanning window function are used. Here,

window size is 70 ms and window overlap value is 20% of the window size. The Short Time Fourier Transform (STFT) spectrogram is calculated using window size 1.4 ms and the overlap value is 95%.

Figures 11 and 12 show the time domain results. A comparison of the simulated vibration, based on model (14), to the experiment is shown for the first 200 ms of vibration. The presented waveforms match up relatively well, given the simplicity of the model (14), especially at the beginning of the vibration. The differences between the presented results (blue lines) are growing with the passage of time which means that all processes not described by model (14) are progressively accumulating. We remind that the dispersion is a progressively accumulating phenomenon. Naturally, we consider two candidates for these unidentified processes: the anomalous dispersion, and the frequency-dependent loss as described by the more realistic full model (3).

Let us consider the possibility of dispersion. We assume that the experimental data has losses similar to (10) of full model (3). The losses associated with the large wavenumbers (see Fig. 7), remain non-dominating for the first periods of vibration, in fact, that is clearly evident in Fig. 12a where the model (14) is almost equal to the experiment. Small differences are present only for the discontinuous edges of the peaks and valleys of the modeled time-series. Not surprisingly, these regions are associated with extremely large wavenumbers κ. As long as we focus on the regions in-between the pointy edges, the losses should be minimal, especially for $t \ll 1$. Figure 12c shows the experimental evidence of the anomalous dispersion. The evolution of the vibration is qualitatively similar to the result shown in Fig. 10. A dispersive high-frequency oscillating tail emerges from the right-hand side of the signal's valley and propagates to the left. This happens for every succeed-
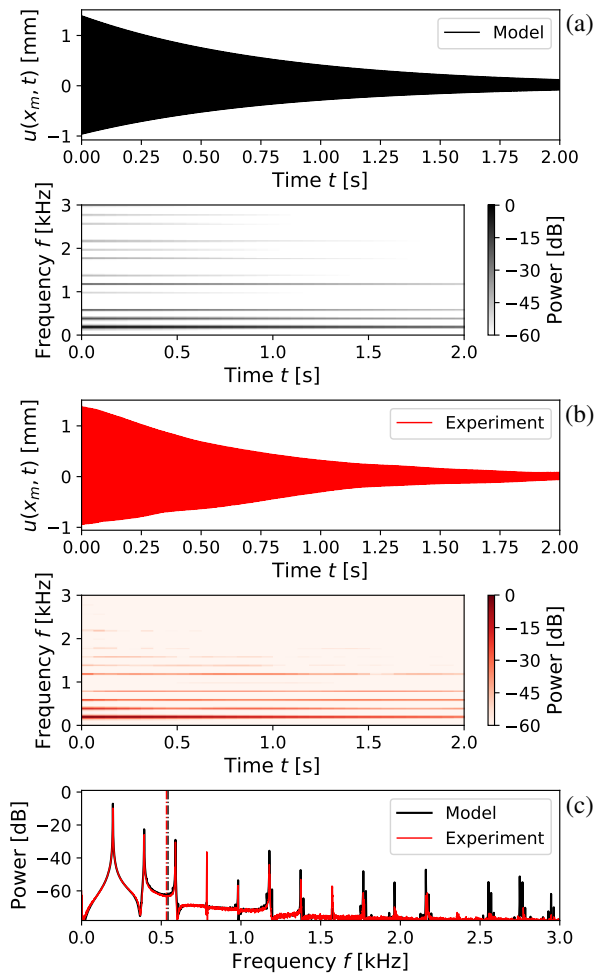
Figure 13. (a) Modeled time-series (14) and the corresponding spectrogram. (b) Time-series and spectrogram of the experiment. (c) Power spectra of the above signals. Spectral centroids are indicated by the dash-dotted lines.
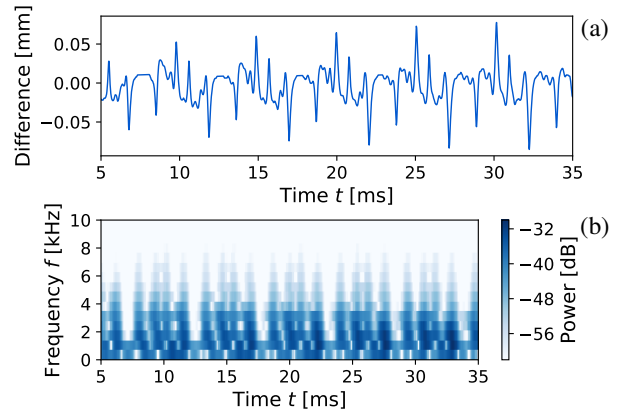

Figure 14. (a) Magnified time-series of the difference between the model (14) and the experiment shown in Fig. 11c. (b) STFT spectrogram of the above signal.

ation is particularly overwhelming for large wavenumber modes, associated with our dispersive oscillating leading tail. This means that with the passage of time, the high-frequency oscillations simply decay much faster compared to the low-frequency modes.

Figure 14 shows another line of evidence for the existence of dispersion. It presents the STFT spectroscopic analysis of the difference signal shown in Fig. 11c. This way of visualising effects of dispersion was suggested by Woodhouse [21]. The window size of 1.4 ms is related to the highest partial present in the signal (≈ 7 kHz). The distinct vertical "formants" can be seen slanting to the left. This result in combination with the time domain result shown in Fig. 12c indicates that high-frequency wave components arrive sooner in comparison to the low-frequency ones.

It is natural to treat the numerical approach presented in Sec. 4 as a digital waveguide and apply digital filters to the traveling waves (18) and (19). All-pass dispersive filters could be used to tune our time-stepping model to the experimental data and thus synthesise realistic sounds [22–24]. If one wishes to remain true to the full model (3) it is possible to derive a digital filter based on it. Bensa *et al.* in [6] show how one can relate the full model to a digital waveguide structure using dispersion relations (10) and (11).

6. CONCLUSIONS

This paper presented results of the experimental study of dispersive wave propagation on guitar strings. The evidence of the dispersion was found and presented. Unsurprisingly, the effect was minor but definitively present.

The high-resolution experimental data of the string displacement was gathered using the video-kymographic high-speed imaging. The experimental data was then compared against the non-dispersive model described by Eq. (14) that was used to identify dispersive features present in experimental data, and to distinguish them from other effects, such as frequency-dependent dissipation shown to be prominent in the more realistic model described by Eq. (3).

The video-kymographic experimental method presented here has proven to be highly reliable for our purposes. We

ing period with the oscillation amplitude becoming progressively larger. Although, the geometry (boundary conditions) of the problem discussed here compared to the one shown in Fig. 10 is different the conclusions regarding the leading high-frequency tail evolution still hold.

Figure 13 shows the frequency domain results. At the beginning of the vibration partial contents of the modeled signal (14), in comparison to the experiment, has higher peaks for $f \gtrsim 1$ kHz. This is most likely due to a combination of the absence of the frequency-dependent attenuation in model (14) and the unrealistic discontinuities present in the initial condition shown in Fig. 5. The decay rate of high-frequency partials, as seen on the spectrograms, is greater for the experimental result which agrees with the dispersion analysis of full model (3). No obvious high-power inharmonic partials are visible in the power spectra shown in Fig. 13c. The identified dispersive wave features present in the experimental data are extremely weak due to the low bending stiffness of the thin guitar string used in the experiment. Additionally, the dispersion is also masked by the frequency-dependent losses. The attenu-

strongly suggest to use this method for measurements of rapidly moving sub-millimetre sized object and displacements in applications where high spatial and temporal resolution of measurement results are required.

Acknowledgments

7. REFERENCES

[1] M. Podlesak and A. R. Lee, "Dispersion of waves in piano strings," *J. Acoust. Soc. Am.*, vol. 83, no. 1, 1988.

[2] L. Hiller and P. M. Ruiz, "Synthesizing musical sounds by solving the wave equation for vibrating objects," *J. Audio Eng. Soc.*, vol. 19, no. 6, pp. 462–551, 1971.

[3] R. Bacon and J. Bowsher, "A discrete model of a struck string," *Acustica*, vol. 41, no. 1, pp. 21–27, 1978.

[4] A. Chaigne, "On the use of finite differences for musical synthesis. Application to plucked stringed instruments," *J. Acoust.*, vol. 5, pp. 181–211, 1992.

[5] A. Chaigne and A. Askenfelt, "Numerical simulations of struck strings. I. A physical model for a struck string using finite difference methods," *J. Acoust. Soc. Am.*, vol. 95, no. 2, pp. 1112–1118, 1994.

[6] J. Bensa, S. Bilbao, R. Kronland-Martinet, and J. O. Smith, "The simulation of piano string vibration: from physical models to finite difference schemes and digital waveguides," *J. Acoust. Soc. Am.*, vol. 114, no. 2, pp. 1095–1107, 2003.

[7] C. Cuesta and C. Valette, "Evolution temporelle de la vibration des cordes de clavecin," *Acustica*, vol. 66, no. 1, pp. 37–45, 1988.

[8] C. Desvages, S. Bilbao, and M. Ducceschi, "Improved frequency-dependent damping for time domain modelling of linear string vibration," in *Proc. 22nd Int. Cong. on Acoust.*, Buenos Aires, Argentina, Sept. 2016, pp. 1–10.

[9] N. H. Fletcher and T. D. Rossing, *The Physics of Musical Instruments*. USA: Springer, 1998.

[10] R. C. D. Paiva, J. Pakarinen, and V. Välimäki, "Acoustics and modeling of pickups," *J. Audio Eng. Soc.*, vol. 60, no. 10, pp. 768–782, 2012.

[11] J. Pakarinen and M. Karjalainen, "An apparatus for measuring string vibration using electric field sensing," in *Proc. Stockholm Music Acoust. Conf.*, Stockholm, Sweden, 2003, pp. 739–742.

[12] J. Kotus, P. Szczuko, M. Szczodrak, and A. Czyżewski, "Application of fast cameras to string vibrations recording," in *2015 Signal Processing: Algorithms, Architectures, Arrangements, and Applications*, Poznan, Poland, September 2015, pp. 104–109.

[13] Y. Achkire and A. Preumont, "Optical measurement of cable and string vibration," *Shock and Vibration*, vol. 5, no. 3, pp. 171–179, 1998.

[14] M. Podlesak and A. R. Lee, "A photovoltaic detector for string vibration measurement," *J. Acoust. Soc. Am.*, vol. 79, no. 6, pp. 2092–2093, 1986.

[15] D. Kartofelev, M. Mustonen, A. Stulov, and V. Välimäki, "Application of high-speed line scan camera for string vibration measurements," in *Proc. Int. Symp. on Musical Acoust.*, Le Mans, France, July 2014, pp. 629–634.

[16] M. Mustonen, D. Kartofelev, A. Stulov, and V. Välimäki, "Application of high-speed line scan camera for acoustic measurements of vibrating objects," in *Proc. 7th Forum Acusticum*, Kraków, Poland, September 2014, pp. 1–6.

[17] M. Mustonen, D. Kartofelev, A. Stulov, and V. Välimäki, "Experimental verification of pickup nonlinearity," in *Proc. Int. Symp. on Musical Acoust.*, Le Mans, France, July 2014, pp. 651–656.

[18] D. Kartofelev, A. Stulov, H.-M. Lehtonen, and V. Välimäki, "Modeling a vibrating string terminated against a bridge with arbitrary geometry," in *Proc. 4th Stockholm Music Acoust. Conf.*, Stockholm, Sweden, Jul. 30–Aug. 3 2013, pp. 626–632.

[19] D. Kartofelev, "Kinematics of ideal string vibration against a rigid obstacle," in *Proc. 20th Int. Conf. on Digital Audio Effects*, Edinburgh, Scotland, UK, September 2017, pp. 40–47.

[20] J. O. Smith, *Physical Audio Signal Processing for Virtual Musical Instruments and Audio Effects*. W3K Publishing, 2010.

[21] J. Woodhouse, "Plucked guitar transients: comparison of measurements and synthesis," *Acta Acust. united Ac.*, vol. 90, no. 5, pp. 945–965, 2004.

[22] J. S. Abel and J. O. Smith, "Robust design of very high-order allpass dispersion filters," in *Proc. Int. Conf. on Digital Audio Effects*, Montreal, Canada, September 2006, pp. 13–18.

[23] J. Rauhala and V. Välimäki, "Tunable dispersion filter design for piano synthesis," *IEEE Signal Processing Letters*, vol. 13, no. 5, pp. 253–256, 2006.

[24] ——, "Dispersion modeling in waveguide piano synthesis using tunable allpass filters," in *Proc. Int. Conf. on Digital Audio Effects*, Montreal, Canada, September 2006, pp. 71–76.